
MSC 2010: 37D20, 37D45, 70G60, 70Q05

Some Mechanical Systems Manifesting Robust Chaos

S. P. Kuznetsov

Three dissipative mechanical systems are considered which manifest chaotic dynamics generated by attractors of Smale – Williams type: (i) motion of a particle on a plane under periodic pulsed kicks, (ii) two interacting particles placed on alternately rotating disks, and (iii) parametric excitation of a string by modulated pump in a finite-dimensional approximation. These examples are interesting as they endow the theory of hyperbolic dynamical systems with clear physically meaningful content.

Keywords: uniformly hyperbolic systems, strange attractors, chaotic dynamics, dynamical systems methods, control of mechanical systems

Introduction

For the past half-century of rapid development of the mathematical theory of dynamical systems many interesting phenomena of complex dynamics have been discovered, but not all of them were considered with respect to real nonlinear systems in applications (mechanics, electronics, nonlinear optics, chemical kinetics).

One type of behavior not discussed for real-world systems for a long time was the structurally stable chaotic dynamics associated with uniformly hyperbolic attractors [1–8], such as the Smale – Williams solenoid.

The mathematical construction for the simplest case of the Smale – Williams attractor is based on a three-dimensional map. Consider a region in the form of a torus in three-dimensional state space; think of it as made of a plastic material. One

Received September 21, 2013

Accepted October 16, 2013

Sergey P. Kuznetsov

alek.art@mail.ru

Kotel'nikov's Institute of Radio-Engineering and Electronics of RAS, Saratov Branch
Zelenaya str., 38, Saratov, 410019, Russian Federation



Fig. 1. Geometric construction of the Smale–Williams attractor. From left to right: the region in the form of a torus in three-dimensional state space, the result of transforming after one and two iterations, and the solenoid obtained in the limit of a large number of repetitions of the transformation.

step of the transformation is that we stretch it twice with simultaneous transversal compression, fold it to form a double loop, and put the loop inside the original torus (Fig. 1). This procedure is repeated many times. At each step the volume of the object decreases (this means that the mapping is dissipative), and the number of turns is doubled, and in the limit tends to infinity. The result is formation of the so-called solenoid, which has Cantor-like structure in the transversal direction. The essential point is that the angular coordinate undergoes doubling at each next discrete time step, namely, $\theta_{n+1} = 2\theta_n \pmod{2\pi}$ (Fig. 1).

An obvious generalization is to carry out the same procedure, but making the loops of another number of coils M . It corresponds to mappings for the angular coordinate $\varphi_{n+1} = M\varphi_n \pmod{2\pi}$. With $M \geq 2$ it is an expanding circle map, or a Bernoulli map.

While mathematicians develop their examples using geometrical, topological, algebraic constructions for building models with structurally stable chaos, a physicist may apply his own specific tool-box and deal with particles, fields, oscillators, feedback loops. Recently, significant progress has been achieved in this respect; numerous examples of physically realizable systems were offered with chaotic attractors of Smale–Williams type and with some other kinds of hyperbolic attractors [9–15].

Regarding clarity and transparency of examples, preference surely should be given to mechanical systems [16–19]. Indeed, the mechanical movements are easily perceived and interpreted from our everyday experience. (In this respect it is worth mentioning an example called the triple linkage, the hinge mechanism manifesting Anosov dynamics that is a type of hyperbolic chaos in conservative systems [20, 21].)

The present article is devoted to consideration and numerical study of several simple mechanical systems with chaotic dynamics associated with attractors of Smale–Williams type. These examples are interesting as they endow the hyperbolic theory of dynamical systems with clear physically meaningful content.

What may be the value of these models from a practical point of view?

The practical application of chaos has attracted attention for many years; numerous international conferences on these issues were organized. In particular, such directions were discussed as secure communication [22, 23], generation of random numbers [24], and application in cryptographic schemes [25]. For mechanical systems, the most interesting feature of chaos is apparently the ability to effectively control the

dynamics by means of arbitrarily small carefully chosen forcing [26]. The possibility of such manipulation with chaotic motions exists due to their fundamentally inherent sensitivity to small perturbations of initial conditions; the corresponding field of studies is referred to as chaos control [27].

Whatever manner of application of chaos we discuss, we should prefer to deal with systems that are robust (rough) or structurally stable, which implies insensitivity of the dynamics to variations of parameters and system characteristics, to technical imperfections, interferences, fluctuations etc. In the theory of oscillations, starting from classical works of Andronov and his research school [5, 6, 28], the rough systems are regarded as those of top-priority for theoretical studies, and as the most important for practice. Traditionally, it relates to systems with regular dynamics, but it seems evident that the same should be true for chaotic systems with uniformly hyperbolic attractors, for which the structural stability is proved mathematically. In this respect examples of systems with uniformly hyperbolic attractors deserve attention and discussion in the context of possible applications of chaos.

1. Particle motion in the plane under periodic kicks

Consider a particle of unit mass on the plane (x, y) in a stationary potential field $U(x, y) = -\frac{1}{2}\mu(x^2 + y^2) + \frac{1}{4}\mu(x^2 + y^2)^2$ possessing rotational symmetry about the origin, with minimum on the unit circle (Fig. 1).¹ We assume that an additional force field with potential $V(x, y) = \frac{1}{2}(x^2 + y^2) - \frac{1}{3}x^3 + xy^2$ is switched on and off periodically with time interval T , producing short-time kicks of magnitude and direction depending on the instantaneous position of the particle. The Lagrange function for this problem is

$$\begin{aligned} L &= \frac{1}{2}(\dot{x}^2 + \dot{y}^2) - U(x, y) - V(x, y) \sum_{n=-\infty}^{\infty} \delta(t - nT) = \\ &= \frac{1}{2}(\dot{x}^2 + \dot{y}^2) + \frac{1}{2}\mu \left[x^2 + y^2 - \frac{1}{2}(x^2 + y^2)^2 \right] + \\ &+ \left(-\frac{1}{2}x^2 - \frac{1}{2}y^2 + \frac{1}{3}x^3 - xy^2 \right) \sum_{n=-\infty}^{\infty} \delta(t - nT). \end{aligned} \quad (1.1)$$

In practice, the potential $V(x, y)$ can be achieved using six electromagnets A-F forming the hexapole and an additional magnet G that creates a centrally symmetric part of the potential (see Figure 2). All these magnets are switched on periodically by current pulses at the same moments of time. The particle should be represented by a permanent magnet, one pole of which is involved in the interaction, and the other one is placed outside the interaction region.

¹The model outlined here is a modification of the model previously discussed in [9, 10, 26], but the present version seems to be better adapted for possible implementation.

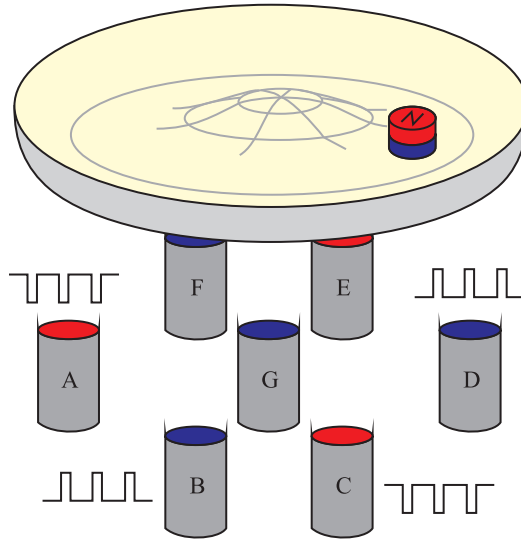


Fig. 2. Schematic setup for the particle motion under periodic kicks modeled by equations (1.2). Gray cylinders are electromagnets switched on periodically by current pulses; the colors of their plane faces indicate the polarity.

The Lagrange equations with an added viscous friction force proportional to the instantaneous velocity read

$$\begin{aligned} \ddot{x} &= \mu x (1 - x^2 - y^2) + (-x + x^2 - y^2) \sum_{n=-\infty}^{\infty} \delta(t - nT) - \alpha \dot{x}, \\ \ddot{y} &= \mu y (1 - x^2 - y^2) + (-y - 2xy) \sum_{n=-\infty}^{\infty} \delta(t - nT) - \alpha \dot{y}, \end{aligned} \quad (1.2)$$

where the coefficient of kinetic friction is assumed to be equal to unity for simplicity: $\alpha = 1$.

Let us explain the functioning of the system. Suppose that initially we have a ring of particles resting on the unit circle with coordinates $x = \cos \varphi$ and $y = \sin \varphi$, where $0 \leq \varphi < 2\pi$. After a kick from the force field V , each particle with initial angle φ will get the momentum components $P_x = -x + x^2 - y^2$ and $P_y = -y - 2xy$. If we still do not take the field U into account, the particles will stop due to friction at the locations with coordinates

$$x' = x + P_x = x^2 - y^2, \quad y' = y + P_y = -2xy. \quad (1.3)$$

Substituting $x = \cos \varphi$ and $y = \sin \varphi$, we obtain $x' = \cos \varphi'$ and $y' = \sin \varphi'$, where $\varphi' = -2\varphi$. This means that the particles settle down again on the unit circle, but a single bypass of the original ring corresponds to a twofold bypass of the newly formed ring in the opposite direction. Thus, for the angular coordinate we have the expanding circle map, or the Bernoulli map.

In equations (1.2) the parameter μ may be selected to be relatively small; then, during the characteristic time of motion caused by a single kick, a displacement of the particle due to the potential field $U(x, y)$ is rather negligible. On the other hand, the period of kicks T is assumed to be large enough to have time for the particle to approach the potential minimum of $U(x, y)$. These conditions are not strong and may be valid at least in a rough approximation. (This is due to structural stability of the hyperbolic attractor we intend to construct.) Given the initial state just before the n -th kick $\mathbf{x}_n = \{x, \dot{x}, y, \dot{y}\}_{t=nT-0}$, one can determine the state before the next, $n + 1$ -th kick from the solution of equations (1.2) on the period T :

$$\ddot{x} + \dot{x} = \mu x (1 - x^2 - y^2), \quad \ddot{y} + \dot{y} = \mu y (1 - x^2 - y^2) \quad (1.4)$$

with initial conditions determined by the state immediately after the kick:

$$\begin{aligned} x|_{t=nT+0} &= x_n, & \dot{x}|_{t=nT+0} &= \dot{x}_n - x_n + x_n^2 - y_n^2, \\ y|_{t=nT+0} &= y_n, & \dot{y}|_{t=nT+0} &= \dot{y}_n - y_n - 2x_n y_n. \end{aligned} \quad (1.5)$$

Relations (1.4) and (1.5) lead to the four-dimensional Poincaré map $\mathbf{x}_{n+1} = \mathbf{f}(\mathbf{x}_n)$. This map is invertible because all the state transformations produced by the kicks and by the continuous time evolution according to the differential equations are invertible. Although the exact form for the map is not derived analytically, the action of this map can be easily reproduced by numerically solving the differential equations (1.4) using a computer program.

The attractor of this map is the Smale – Williams solenoid because of the outlined topological property of the ensemble of particles after the conversion, namely, the emergence of the loop bypassing the origin twice. Transversal compression in the phase space occurs due to the friction of the particle during the motion between the kicks in the potential field U towards the potential minimum on the unit circle. In contrast to the classical construction mentioned in the introduction, the Smale – Williams attractor in this model is embedded into the four-dimensional (rather than three-dimensional) phase space.

Figures 3–5 illustrate results of the numerical solutions of equations (1.2). Figure 3 depicts a typical trajectory of a particle during the course of its motion and a portrait of the attractor in the stroboscopic section in projection onto the plane (x, y) . The attractor obviously looks like a kind of Smale – Williams solenoid, with distinguishable Cantor-like transversal structure. Figure 4 shows the iterative diagram for the angular variable $\varphi_n = \arg(x(nT - 0) + iy(nT - 0))$ determined immediately before each successive kick. One can see that the angular coordinate behaves in accordance with the expanding circle map, or the Bernoulli map. One bypass of the circle for the pre-image implies two detours for the image in the opposite direction.

In dynamical systems theory, to describe the behavior near a reference phase trajectory Lyapunov exponents are introduced, which characterize departure (the positive exponents) or approach (the negative exponents) to the reference trajectory. The total number of the exponents corresponds to the dimension of the phase space, so there are four of them for the Poincaré map of the system (1.2). The standard

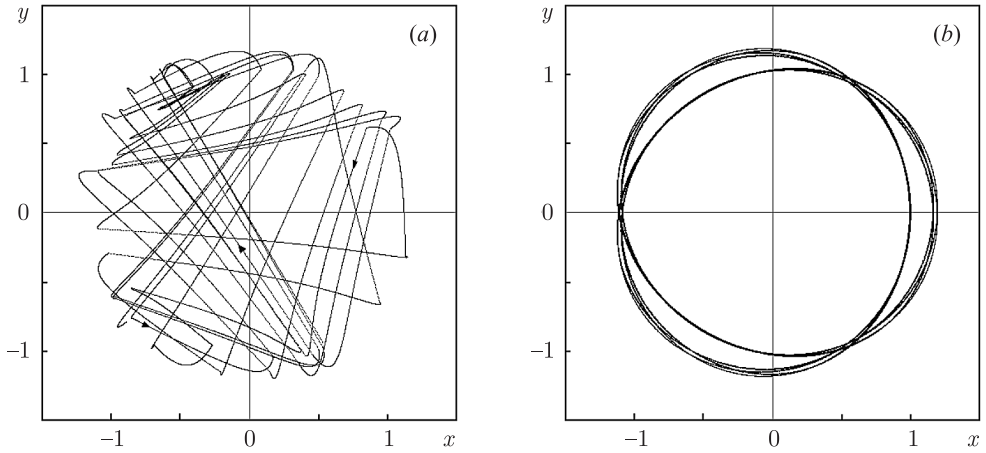


Fig. 3. A trajectory of the particle in the plane (x, y) in the model (1.2) with $\mu = 0.3$, $T = 4$ for 50 periods of the pulse driving, where the arrows indicate directions of the motion (a), and a portrait of the attractor in the stroboscopic cross-section (b).

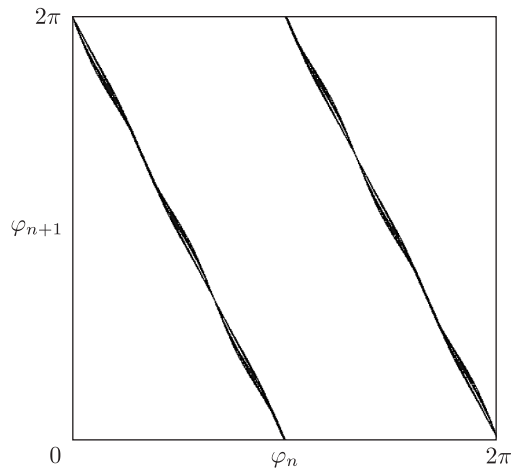


Fig. 4. Iteration diagram for the angular variable obtained from the numerical solutions of equations (1.2) at $\mu = 0.3$, $T = 4$.

approach to computation of the exponents is the method of Benettin [30–32]. In our particular case it is based on numerical solution of equation (1.4) for the reference orbit taking into account (1.5) at the kicks and simultaneous solution of a collection of four replicas of variation equations with Gram–Schmidt orthogonalization and normalization of the perturbation vectors after each kick. At $\mu = 0.3$ and $T = 4$ the Lyapunov exponents for the Poincaré map are

$$\Lambda_1 = 0.687, \quad \Lambda_2 = -1.386, \quad \Lambda_3 = -3.000, \quad \Lambda_4 = -3.733. \quad (1.6)$$

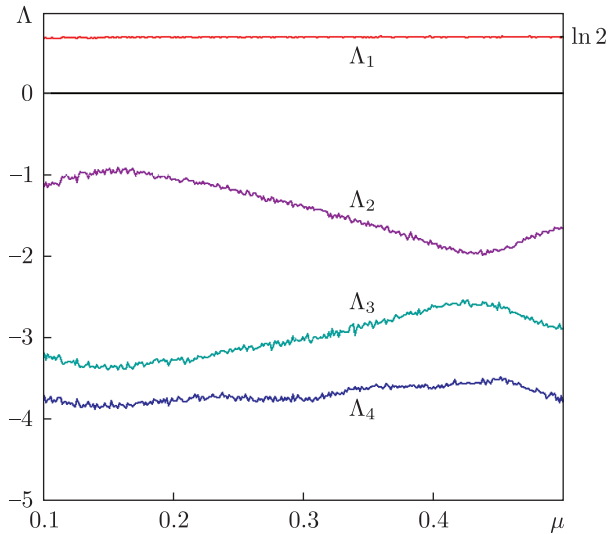


Fig. 5. The Lyapunov exponents of the Poincaré map for the model (1.2) versus μ at $T = 4$.

Figure 5 plots the Lyapunov exponents depending on the parameter μ for a fixed T . Note that the largest Lyapunov exponent for the stroboscopic map remains approximately constant and very close to $\ln 2$. This value corresponds to the Bernoulli map, approximately describing the dynamics of the angular variable. The remaining Lyapunov exponents are negative.

As noted in the introduction, the essential attribute of the Smale–Williams attractor is the inherent Cantor-like transversal structure. To characterize this structure, one can estimate the fractal dimension. Kaplan and Yorke proposed a formula that expresses the dimension via the Lyapunov exponents approximately [31–33]. It reads

$$D_{KY} = m + S_m / |\Lambda_{m+1}|, \quad S_m = \sum_{i=1}^m \Lambda_i. \tag{1.7}$$

Here the Lyapunov exponents $\Lambda_1, \dots, \Lambda_m, \dots, \Lambda_N$ are numbered in descending order, and m is an integer such that the sum S_m is positive, but S_{m+1} is negative. Empirically, this formula gives results close to the properly defined fractal dimensions of attractors, although it has no rigorous mathematical basis and proof. Therefore, it is commonly used to regard the estimate (1.7) as a special kind of dimension, called the Kaplan–Yorke dimension or the Lyapunov dimension. Note that the heuristic derivation of (1.7) suggests uniform compressions and expansions of the phase volume in some directions in the course of the dynamical evolution on the attractor, and this assumption is justified in the best degree just for the uniformly hyperbolic attractors.

The estimate of the attractor dimension for the Poincaré section of the system (1.2) at $\mu = 0.3$, $T = 4$ according to the Kaplan–Yorke formula yields $D = 1.50$.

2. A system of two interacting particles placed on alternately rotating disks

Consider two disks disposed horizontally, one above the other, which rotate about the common axis alternately (while one rotates, the other is at rest and vice versa) with angular velocity ω (Figure 1, *a*). On each disk a particle is placed which is capable of sliding on it with the friction force proportional to its velocity relative to the disk. Suppose that there is a potential field $U(r)$ symmetric about the axis, with potential minimum at the center and strongly growing to the edges of the disks. In addition, assume that the two particles interact via a potential field $V(\mathbf{r}_1 - \mathbf{r}_2)$, where \mathbf{r}_1 and \mathbf{r}_2 are the position vectors. As will be seen, under appropriate choice of the potential functions and other parameters, in the map which describes the state transformation on successive periods of the rotation switching, the chaotic dynamics corresponding to the attractor of Smale–Williams type will take place.

Let us set²

$$U(x, y) = \frac{1}{2}k(x^2 + y^2) + \frac{1}{4}(x^2 + y^2)^2 \quad (2.1)$$

and

$$V(x, y) = -\frac{1}{3}x^3 + xy^2. \quad (2.2)$$

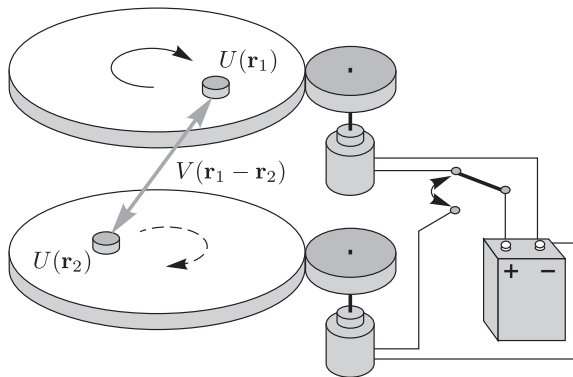


Fig. 6. Scheme of possible design implementing the motion of two interacting particles on alternately rotating disks, modeled by equations (2.5).

²Practically the potential field (2.1) may be implemented by replacing the plane disks by cup-shaped surfaces, and the potential (2.2) using a single magnet for the first particle, and the hexapole construction of magnets instead the second one (its spatial orientation should remain unchanged in the course of time evolution, regardless of the rotation of the disk). In the formal description, we do not focus on this particular implementation, because it masks the inherent symmetry between two components of the model system.

In the absence of friction, the system is characterized by the Lagrange function

$$L = \sum_{i=1}^2 \left[\frac{1}{2} (\dot{x}_i^2 + \dot{y}_i^2) - \frac{1}{2} k (x_i^2 + y_i^2) - \frac{1}{4} (x_i^2 + y_i^2)^2 \right] + \frac{1}{3} (x_1 - x_2)^3 - (x_1 - x_2)(y_1 - y_2)^2, \tag{2.3}$$

where $x_{1,2}, y_{1,2}$ are Cartesian coordinates of the particles on their disks, $u_{1,2}$ and $v_{1,2}$ are two corresponding generalized momenta, k is a parameter. To take into account the viscous friction in the corresponding Lagrange equations, we must add terms proportional to velocities of the particles relative to the disks. On the disk rotating with angular velocity ω the instant velocity at the particle position (x_i, y_i) is $\mathbf{v} = (-\omega y_i, \omega x_i)$; so, we obtain

$$\begin{aligned} \frac{d}{dt} \frac{\partial L}{\partial \dot{x}_1} &= \frac{\partial L}{\partial x_1} - \alpha \left(\frac{dx_1}{dt} + \omega_1 y_1 \right), \\ \frac{d}{dt} \frac{\partial L}{\partial \dot{y}_1} &= \frac{\partial L}{\partial y_1} - \alpha \left(\frac{dy_1}{dt} - \omega_1 x_1 \right), \\ \frac{d}{dt} \frac{\partial L}{\partial \dot{x}_2} &= \frac{\partial L}{\partial x_2} - \alpha \left(\frac{dx_2}{dt} + \omega_2 y_2 \right), \\ \frac{d}{dt} \frac{\partial L}{\partial \dot{y}_2} &= \frac{\partial L}{\partial y_2} - \alpha \left(\frac{dy_2}{dt} - \omega_2 x_2 \right), \end{aligned} \tag{2.4}$$

or

$$\begin{aligned} \ddot{x}_1 &= -x_1 (k + x_1^2 + y_1^2) + \alpha (-\omega_1 y_1 - \dot{x}_1) - \varepsilon [(x_1 - x_2)^2 - (y_1 - y_2)^2], \\ \ddot{y}_1 &= -y_1 (k + x_1^2 + y_1^2) + \alpha (\omega_1 x_1 - \dot{y}_1) + 2\varepsilon (x_1 - x_2)(y_1 - y_2), \\ \ddot{x}_2 &= -x_2 (k + x_2^2 + y_2^2) + \alpha (-\omega_2 y_2 - \dot{x}_2) + \varepsilon [(x_1 - x_2)^2 - (y_1 - y_2)^2], \\ \ddot{y}_2 &= -y_2 (k + x_2^2 + y_2^2) + \alpha (\omega_2 x_2 - \dot{y}_2) - 2\varepsilon (x_1 - x_2)(y_1 - y_2), \end{aligned} \tag{2.5}$$

where

$$\omega_1(t) = \begin{cases} \omega_0, & nT \leq t < nT + T/2, \\ 0, & nT + T/2 \leq t < nT, \end{cases} \quad \omega_2(t) = \begin{cases} 0, & nT \leq t < nT + T/2, \\ \omega_0, & nT + T/2 \leq t < nT. \end{cases} \tag{2.6}$$

Figure 7 illustrates a typical dynamical regime of the model obtained from the numerical solution of equations (2.5) at

$$k = 3, \quad \alpha = 3, \quad \varepsilon = 0.03, \quad T = 16, \quad \omega_0 = 2\pi. \tag{2.7}$$

The diagrams show the time evolution of the spatial position of the particles in the course of operation of the system. Observe that motions of the individual particles take place alternately, and the motion is not periodic: the forms of the orbits are not repeated in successive stages of activity.

Figure 8 shows an iteration diagram for the angular coordinate $\varphi_n = \arg(x(nT - 0) + iy(nT - 0))$ of one of the particles, determined immediately after the end of each

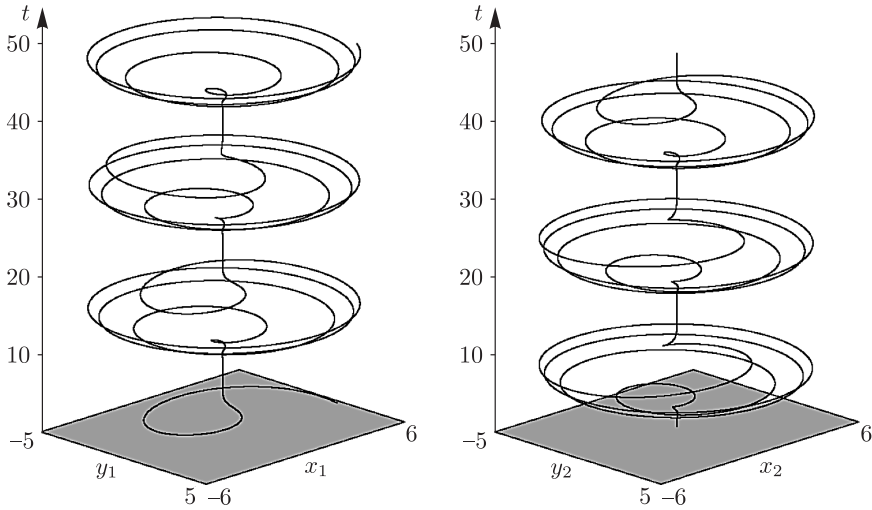


Fig. 7. Time evolution of the spatial position of the particles on the disks during the operation of the model (2.5) with parameters (2.7).

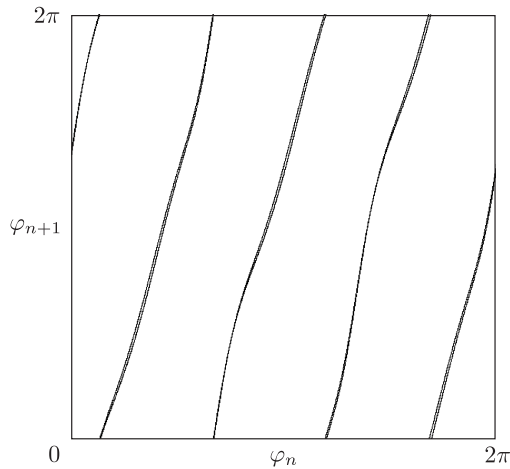


Fig. 8. The iteration diagram for the angular coordinates of one of the particles obtained from the numerical solution of equations (2.5) with parameters (2.7).

rotation stage of the corresponding disk. Observe that the angular coordinate behaves in accordance with the expanding circle map or the Bernoulli map. One bypass around the circle for the pre-image implies four bypasses for the image. Figure 9 shows the attractor in the stroboscopic section in projection onto the plane of coordinates of one particle (x_1, y_1) . In the original scale, it looks like a circle, but a zoom reveals a distinguishable Cantor-like structure intrinsic to the Smale–Williams solenoid as

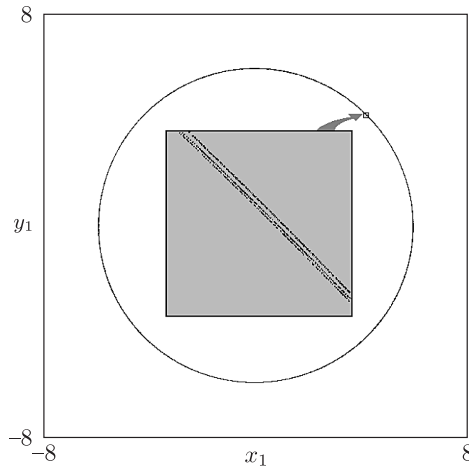


Fig. 9. Attractor in the stroboscopic section for the model given by equations (2.5) with parameters (2.7); observe transversal Cantor structure visible in the inset.

illustrated in the insert. In the present case, the attractor corresponds to a four-time folding of the toroidal domain in the eight-dimensional phase space of the stroboscopic Poincaré map.

Figure 10 shows plots of the Lyapunov exponents versus the parameter of angular velocity of the disks ω . The Lyapunov exponents are calculated by numerically solving equations (2.5) for the reference orbit, together with eight replicas of the variation equations. At each step of integration of the differential equations the Gram – Schmidt orthogonalization of the vectors is carried out. The positive Lyapunov exponent for

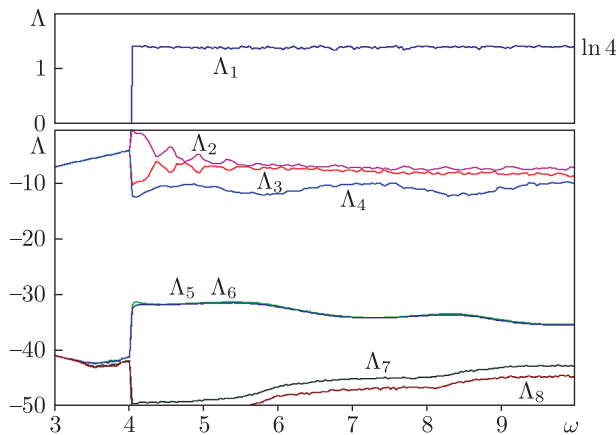


Fig. 10. Lyapunov exponents of the Poincaré map for the model (2.5) versus the angular velocity of the disks' rotations. Other parameters: $k = 3$, $\alpha = 3$, $\varepsilon = 0.03$, $T = 16$.

the stroboscopic map remains approximately constant in a wide parameter range being very close to $\ln 4$ which corresponds to the Bernoulli map, approximately describing the dynamics of the angular variable. In particular, at $\omega = 2\pi$ the Lyapunov exponents are

$$\begin{aligned} \Lambda_1 &= 1.354, & \Lambda_2 &= -6.90, & \Lambda_3 &= -7.65, & \Lambda_4 &= -11.61, \\ \Lambda_5 &= -32.81, & \Lambda_6 &= -32.92, & \Lambda_7 &= -45.34, & \Lambda_8 &= -47.26. \end{aligned} \quad (2.8)$$

The fractal dimension by the Kaplan–Yorke formula for this attractor is $D \approx 1.20$.

3. Hyperbolic chaos in parametric oscillations of a string

It is known that string vibration is governed by the partial differential equation [34]

$$\rho \frac{\partial^2 y}{\partial t^2} = G \frac{\partial^2 y}{\partial x^2}, \quad (3.1)$$

where $y(x, t)$ is the transversal displacement of the string at the point x at time t , ρ is the linear density of the string (mass per unit length), G is the tension force. For a uniform string with a constant tension, the value $c = \sqrt{G/\rho}$ determines the speed of the wave propagation.

The string of length L with fixed ends has a set of modes with natural frequencies $\omega_s = \pi s c/L$. In the classic Melde experiment [34, 35] periodic variation of the string tension with frequency $2\omega_0$ acts as a pump for the parametric oscillations of the appropriate standing-wave mode of frequency ω_0 (Figure 11). The initial stage of the oscillation growth is described by (3.1), where the coefficient G is represented by a function of time; for example, it may be specified as $G = G_0(1 + a_2^0 \sin 2\omega_0 t)$, $a_2^0 < 1$.

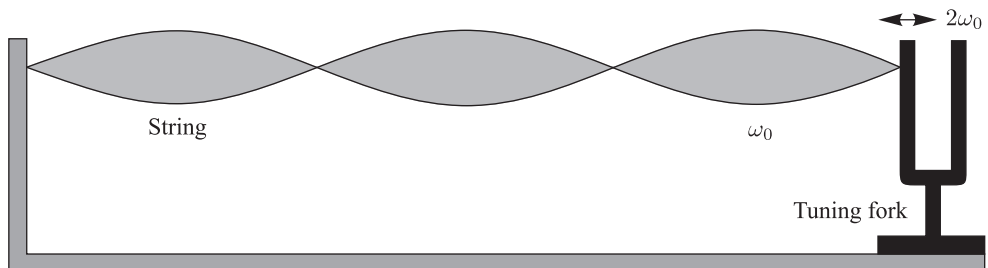


Fig. 11. The Melde experiment (1859): periodic variation of the string tension due to the tuning fork vibration of frequency $2\omega_0$ causes the parametric excitation of the standing-wave mode of frequency ω_0 .

Recently a way was suggested to modify the setup of the string parametric excitation to produce chaotic oscillations associated with the structurally stable attractor of Smale–Williams type [36, 37]. The idea is that the pumping alternately on a low and a high frequency will provide the parametric excitation of short and long standing-wave patterns turn by turn. Then, using proper nonlinearity and spatial inhomogeneity we can arrange the transfer of the spatial phase from one pattern to another and back in such a way that a tripling of the phase occurs over the full period of the pump modulation. In the presence of dissipation, compression of the phase volume in the state space ensures the presence of the attractor of Smale–Williams type. The easiest way to implement this idea on the level of a mathematical model relates to a system closed in a ring (although in the experiment it is not the simplest setup to deal with). Here we consider the reduction of the problem with periodic boundary conditions to a finite-dimensional model, the study of which is easier than that for the original distributed system [36, 37].

Suppose that the force of the string tension in (3.1) is expressed as

$$G(t) = G_0 \cdot [1 + a_2(t) \sin 2\omega_0 t + a_6(t) \sin 6\omega_0 t], \quad (3.2)$$

and assume that the coefficients a_2, a_6 vary in time with period T , being alternately large or close to zero. Specifically, we set

$$a_2(t) = a_2^0 \sin^2 \pi(t/T - 1/4), \quad a_6(t) = a_6^0 \cos^2 \pi(t/T - 1/4), \quad (3.3)$$

where non-negative constants a_2^0, a_6^0 satisfy $a_2^0 + a_6^0 < 1$. Thus, the pump has the components at frequencies $2\omega_0$ and $6\omega_0$ with amplitudes, modulated in time. The distribution of mass on the string will be weakly nonuniform, depending on the spatial coordinate as

$$\rho(x) = \rho_0(1 + \varepsilon \sin 4k_0 x), \quad (3.4)$$

where $k_0 = \omega_0/c_0$, $c_0 = \sqrt{G_0/\rho_0}$. In addition, we introduce dissipation by the term $-(\alpha + \beta u^2)\partial y/\partial t$ added to the right-hand side of the equation. The parameter α is responsible for linear dissipation and the parameter β accounts for nonlinear dissipation. The presence of nonlinear dissipation is needed to stabilize the parametric instability; moreover, for the system in question it is also important that the cubic nonlinearity provides generation of the third harmonic in the wave-oscillatory motion. Finally, we add a linear term $-\gamma y$ to ensure damping for the disturbances with wave number about zero. Physically, this term may be interpreted as presence of a potential field, depending on the transversal coordinate, $U(y) = \gamma y^2/2$.

Using appropriate normalization of variables and parameters such that $c_0 = 1$, $k_0 = \omega_0$, $\beta = 1$, we arrive at the partial differential equation of the following form [36, 37]:

$$(1 + \varepsilon \sin 4k_0 x) \frac{\partial^2 y}{\partial t^2} = -(\alpha + y^2) \frac{\partial y}{\partial t} - \gamma y + [1 + a_2^0 \sin^2 \pi(t/T - 1/4) \sin 2\omega_0 t + a_6^0 \cos^2 \pi(t/T - 1/4) \sin 6\omega_0 t] \frac{\partial^2 y}{\partial x^2}. \quad (3.5)$$

Let us impose the periodic boundary conditions

$$y(L, t) = y(0, t), \quad y_x(L, t) = y_x(0, t) \quad (3.6)$$

and select the length L containing an integer number of the wavelengths of the wave number k_0 : $L = 2\pi N/k_0$.

The mechanism of functioning of the system is as follows.

At the stage of pumping at the frequency $2\omega_0$ a standing wave with frequency ω_0 and wave number k_0 is parametrically generated, whose disposition of nodes and antinodes is characterized by a spatial phase θ , roughly $y \sim \cos \omega_0 t \sin(k_0 x + \theta)$. The wave amplitude saturates at some finite level due to the nonlinear dissipation; moreover, the oscillatory-wave motion will contain the third harmonic component: $y_3 \sim \sin 3\omega_0 t \sin(3k_0 x + 3\theta)$.

When the pumping at $2\omega_0$ ceases, the oscillations at frequency ω_0 decay, but now the pumping at $6\omega_0$ starts, which provides the parametric instability for the standing wave pattern of the frequency $3\omega_0$ and the wave number $3k_0$. This process is initiated by the perturbation given by the above expression for y_3 , so it inherits the spatial phase 3θ .

At the next stage of the pumping resumption at $2\omega_0$ the excitation of the standing wave with the frequency ω_0 and the wave number k_0 restarts; it develops in the presence of the seed perturbation determined by combination of the component $y \sim \sin 3\omega_0 t \sin(3k_0 x + 3\theta)$ remaining from the previous stage, and of the component $\varepsilon a_2 \sin 2\omega_0 t \sin 4k_0 x$ present due to the spatially nonuniform mass distribution; it can be expressed as $\sin 2\omega_0 t \sin 3\omega_0 t \sin 4k_0 x \sin(3k_0 x + 3\theta) = -\frac{1}{4} \sin \omega_0 t \cos(k_0 x - 3\theta) + \dots$

It follows that the new phase value θ' is related to the previous one by the expanding circle map $\theta' = -3\theta + \text{const}$ that is the Bernoulli map with chaotic dynamics characterized by a positive Lyapunov exponent $\Lambda = \ln 3 \approx 1.0986$. In other directions compression of the phase volume will occur resulting in formation of the Smale–Williams solenoid in the phase space of the map, which describes the state transformation over the period of pump modulation.

Taking into account that the parametric excitation takes place at the wave numbers k_0 and $3k_0$, to compose the low-dimensional model it is appropriate to use the ansatz

$$y(x, t) = u_1(t) \cos k_0 x + v_1(t) \sin k_0 x + u_3(t) \cos 3k_0 x + v_3(t) \sin 3k_0 x. \quad (3.7)$$

Substituting this in (3.5), we multiply both sides of the equation by $\cos k_0 x$, $\sin k_0 x$, $\cos 3k_0 x$ and $\sin 3k_0 x$, each time performing integration over the spatial period. As a result, we obtain a set of equations for the coefficients

$$\ddot{u}_1 + \frac{1}{2} \varepsilon \ddot{v}_3 = f_1, \quad \ddot{u}_3 + \frac{1}{2} \varepsilon \ddot{v}_1 = f_3, \quad \ddot{v}_1 + \frac{1}{2} \varepsilon \ddot{u}_3 = g_1, \quad \ddot{v}_3 + \frac{1}{2} \varepsilon \ddot{u}_1 = g_3, \quad (3.8)$$

where

$$\begin{aligned}
 f_1 = & -\omega_0^2 (1 + a_2(t) \sin 2\omega_0 t + a_6(t) \sin 6\omega_0 t) u_1 - \gamma u_1 - \alpha \dot{u}_1 - \\
 & - \frac{1}{2} \left[\left(\frac{3}{2} u_1^2 + u_1 u_3 + u_3^2 + \frac{1}{2} v_1^2 + v_1 v_3 + v_3^2 \right) \dot{u}_1 + \right. \\
 & \left. + \frac{1}{2} (u_1^2 + 4u_1 u_3 - v_1^2) \dot{u}_3 + (u_1 v_1 - u_3 v_1 + u_1 v_3) \dot{v}_1 + (u_1 v_1 + 2u_1 v_3) \dot{v}_3 \right], \tag{3.9}
 \end{aligned}$$

$$\begin{aligned}
 g_1 = & -\omega_0^2 (1 + a_2(t) \sin 2\omega_0 t + a_6(t) \sin 6\omega_0 t) v_1 - \gamma v_1 - \\
 & - \alpha \dot{v}_1 - \frac{1}{2} \left[\left(\frac{3}{2} v_1^2 - v_1 v_3 + v_3^2 + \frac{1}{2} u_1^2 - u_1 u_3 + u_3^2 \right) \dot{v}_1 + \right. \\
 & \left. + \frac{1}{2} (u_1^2 + 4v_1 v_3 - v_1^2) \dot{v}_3 + (u_1 v_1 - u_3 v_1 + u_1 v_3) \dot{u}_1 + (-u_1 v_1 + 2u_3 v_1) \dot{u}_3 \right], \tag{3.10}
 \end{aligned}$$

$$\begin{aligned}
 f_3 = & -9\omega_0^2 (1 + a_2(t) \sin 2\omega_0 t + a_6(t) \sin 6\omega_0 t) u_3 - \gamma u_3 - \alpha \dot{u}_3 - \\
 & - \frac{1}{4} [(u_1^2 + 4u_1 u_3 - v_1^2) \dot{u}_1 + 2(-u_1 v_1 + 2u_3 v_1) \dot{v}_1 + \\
 & + (2u_1^2 + 2v_1^2 + 3u_3^2 + v_3^2) \dot{u}_3 + 2u_3 v_3 \dot{v}_3], \tag{3.11}
 \end{aligned}$$

$$\begin{aligned}
 g_3 = & -9\omega_0^2 (1 + a_2(t) \sin 2\omega_0 t + a_6(t) \sin 6\omega_0 t) v_3 - \gamma v_3 - \alpha \dot{v}_3 - \\
 & - \frac{1}{4} [2(u_1 v_1 + 2u_1 v_3) \dot{u}_1 + (u_1^2 + 4v_1 v_3 - v_1^2) \dot{v}_1 + 2u_3 v_3 \dot{u}_3 + \\
 & + (2u_1^2 + 2v_1^2 + u_3^2 + 3v_3^2) \dot{v}_3]. \tag{3.12}
 \end{aligned}$$

The equations may be rewritten in a form more convenient for numerical solution expressing the second derivatives explicitly:

$$\begin{aligned}
 \ddot{u}_1 = \frac{f_1 - \frac{1}{2} \varepsilon g_3}{1 - \frac{1}{4} \varepsilon^2}, & \quad \ddot{u}_3 = \frac{f_3 - \frac{1}{2} \varepsilon g_1}{1 - \frac{1}{4} \varepsilon^2}, \\
 \ddot{v}_1 = \frac{g_1 - \frac{1}{2} \varepsilon f_3}{1 - \frac{1}{4} \varepsilon^2}, & \quad \ddot{v}_3 = \frac{g_3 - \frac{1}{2} \varepsilon f_1}{1 - \frac{1}{4} \varepsilon^2}. \tag{3.13}
 \end{aligned}$$

Figure 12 shows plots of amplitude coefficients versus time, obtained by numerical solution of equations (3.13) at

$$\begin{aligned}
 \omega_0 = 2\pi, \quad k_0 = 2\pi, \quad T = 40, \quad L = 1, \\
 a_2^0 = 0.4, \quad a_6^0 = 0.2, \quad \varepsilon = 0.2, \quad \alpha = 0.4, \quad \gamma = 0.03. \tag{3.14}
 \end{aligned}$$

As can be seen, the relations between the amplitudes of the sine and cosine components (which are associated with the spatial phases of the standing wave patterns) vary chaotically from one period of modulation to another. We introduce the angular variable $\theta_n = \arg [u_1(nT) + iv_1(nT)]$ to characterize the spatial phase at $t = nT$. Figure 13, *a* shows the triple expanding circle map for the phase variable in coordinates

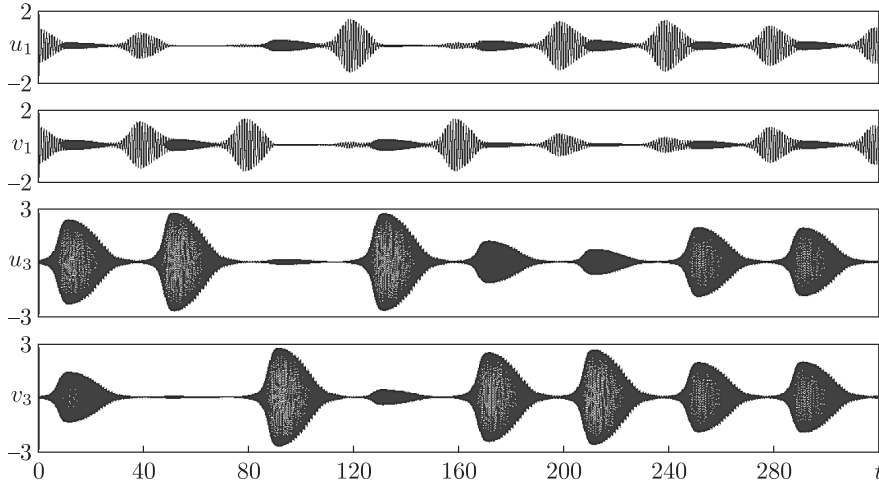


Fig. 12. Plots of the amplitude coefficients versus time, obtained from numerical solution of equations (3.13) with parameters assigned according to (3.14).

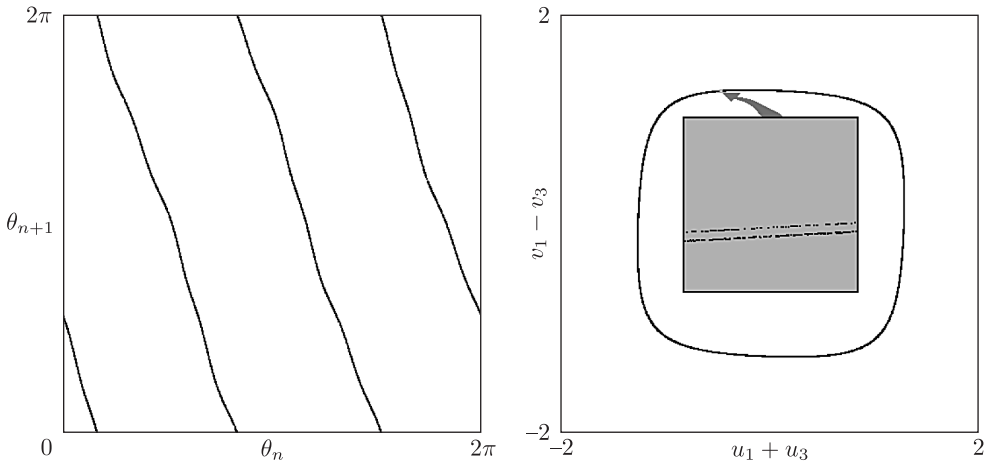


Fig. 13. The diagram for the angular variable responsible for the amplitude ratio for cosine and sine components (a) and the stroboscopic portrait of the attractor in projection onto the plane of variables $u_1 + u_3$ and $v_1 - v_3$ (b); observe a transversal Cantor structure visible in the inset.

(θ_n, θ_{n+1}) . Figure 13, b is a stroboscopic portrait of the attractor in the plane of variables $(u_1 + u_3, v_1 - v_3)$. (To explain the sense of these variables, observe that according to (3.7) $y(0, t) = u_1(t) + u_3(t)$, $y(L/4, t) = v_1(t) + v_3(t)$.)

As the model is represented by a non-autonomous system of equations of the eighth order, the full spectrum of Lyapunov exponents of the Poincaré map contains eight terms. Calculation of the exponents is carried out using the Benettin algorithm.

Setting the parameters according to (3.14), we obtain

$$\begin{aligned} \Lambda_1 &= 1.109, & \Lambda_2 &= -9.544, & \Lambda_3 &= -14.663, & \Lambda_4 &= -23.24, \\ \Lambda_5 &= -27.16, & \Lambda_6 &= -27.97, & \Lambda_7 &= -34.26, & \Lambda_8 &= -41.84. \end{aligned} \tag{3.15}$$

The value of the fractal dimension of the attractor by the Kaplan–Yorke formula in this model is $D \approx 1.12$.

Figure 14 plots the Lyapunov exponents versus parameter of linear dissipation α for other parameters fixed according to (3.14). The leading Lyapunov exponent remains approximately constant for the stroboscopic map, being very close to $\ln 3$. It corresponds to the Bernoulli map, approximately describing the dynamics of the angular variable.

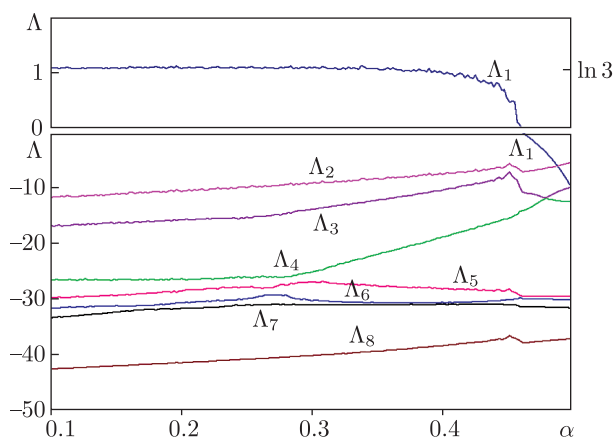


Fig. 14. Plot of the Lyapunov exponents for the finite-dimensional model of the parametrically excited string (3.13) depending on the dissipation parameter α . Other parameters: $\omega_0 = 2\pi$, $k_0 = 2\pi$, $T = 40$, $L = 1$, $a_2^0 = 0.4$, $a_6^0 = 0.2$, $\varepsilon = 0.2$, $\gamma = 0.03$.

The results of calculations based on the finite-dimensional model are in very good agreement with those reported for the direct numerical solution of partial differential equations [36, 37]. However, there is a difference in that some extra negative Lyapunov exponents appear in the spectrum of the distributed system. They are apparently associated with perturbations in the partial differential equation model excluded when using the substitution (3.7). Accordingly, the estimates of attractor dimension by the Kaplan–Yorke formula are also different for the distributed and the low-dimensional model.

Conclusion

The paper presents three examples of mechanical dissipative systems realizing chaotic dynamics caused, as believed, by the presence of attractors of Smale–Williams type. The relative simplicity of the devices and of their principle of operation allows

us to hope that they can be implemented in experiments. Due to the structural stability of chaos associated with the uniformly hyperbolic attractors, the feasibility of the models should not critically depend on details of the constructions, details of distributions of the fields in the first two models, or of exact shape of the pump function and of the spatial inhomogeneity in the third model.

In the framework of the present work, the main evidence for the presence of attractors of Smale–Williams type is the topological nature of the iterative diagrams for angular variables of all three models corresponding to expanding circle maps. At present, arguments in favor of the hyperbolic nature of the attractors are based on qualitative analysis and numerical results. A more accurate mathematical justification for the hyperbolicity, such as verification of the cone criterion and of absence of manifold tangencies [39–41] would be desirable. This may be one of the directions for future studies.

This work was supported by RFBR grant № 12-02-00342.

References

- [1] Smale, S., Differentiable Dynamical Systems, *Bull. Amer. Math. Soc. (NS)*, 1967, vol. 73, pp. 747–817.
- [2] Williams, R. F., Expanding Attractors, *Publ. Math. Inst. Hautes Études Sci.*, 1974, vol. 43, pp. 169–203.
- [3] *Dynamical Systems: Vol. 9. Dynamical Systems with Hyperbolic Behaviour*, D. V. Anosov (Ed.), Encyclopaedia Math. Sci., vol. 66, Berlin: Springer, 1995.
- [4] Katok, A. and Hasselblatt, B., *Introduction to the Modern Theory of Dynamical Systems*, Cambridge: Cambridge Univ. Press, 1995.
- [5] Shilnikov, L. P., Shilnikov, A. L., Turaev, D. V., and Chua L. O., *Methods of Qualitative Theory in Nonlinear Dynamics: Part 1*, World Sci. Ser. Nonlinear Sci. Ser. A Monogr. Treatises, vol. 4, River Edge, NJ: World Scientific, 1998.
- [6] Shilnikov, L. P., Shilnikov, A. L., Turaev, D. V., and Chua L. O., *Methods of Qualitative Theory in Nonlinear Dynamics: Part 2*, World Sci. Ser. Nonlinear Sci. Ser. A Monogr. Treatises, vol. 5, River Edge, NJ: World Scientific, 2001.
- [7] Afraimovich, V. and Hsu, S.-B., *Lectures on Chaotic Dynamical Systems*, AMS/IP Stud. in Adv. Math., vol. 28, Providence, RI: AMS, 2003.
- [8] Bonatti, C., Díaz, L. J., and Viana, M., *Dynamics beyond Uniform Hyperbolicity: A Global Geometric and Probabilistic Perspective*, Encyclopaedia Math. Sci., vol. 102, Berlin: Springer, 2005.
- [9] Kuznetsov, S. P., *Hyperbolic Chaos: A Physicist's View*, Berlin: Springer, 2012.
- [10] Kuznetsov, S. P., Dynamical Chaos and Uniformly Hyperbolic Attractors: From Mathematics to Physics, *Uspekhi Fiz. Nauk*, 2011, vol. 181, pp. 121–149 [*Phys. Uspekhi*, 2011, vol. 54, no. 2, pp. 119–144].
- [11] Kuznetsov, S. P., Example of a Physical System with a Hyperbolic Attractor of the Smale–Williams Type, *Phys. Rev. Lett.*, 2005, vol. 95, no. 14, 144101, 4 pp.
- [12] Isaeva, O. B., Jalnina, A. Yu., and Kuznetsov, S. P., Arnold's Cat Map Dynamics in a System of Coupled Nonautonomous van der Pol Oscillators, *Phys. Rev. E*, 2006, vol. 74, no. 4, 046207, 5 pp.

- [13] Kuznetsov, S. P. and Seleznev, E. P., A Strange Attractor of the Smale–Williams Type in the Chaotic Dynamics of a Physical System, *Zh. Eksp. Teoret. Fiz.*, 2006, vol. 129, no. 2, pp. 400–412 [*J. Exp. Theor. Phys.*, 2006, vol. 102, no. 2, pp. 355–364].
- [14] Kuznetsov, S. P. and Pikovsky, A., Autonomous Coupled Oscillators with Hyperbolic Strange Attractors, *Phys. D*, 2007, vol. 232, no. 2, pp. 87–102.
- [15] Kuznetsov, S. P. and Ponomarenko, V. I., Realization of a Strange Attractor of the Smale–Williams type in a Radiotechnical Delay-Fedback Oscillator, *Tech. Phys. Lett.*, 2008, vol. 34, no. 9, pp. 771–773.
- [16] Arnold, V. I. and Avez, A., *Ergodic Problems in Classical Mechanics*, New York: Benjamin, 1968.
- [17] Borisov, A. V. and Mamaev, I. S., Strange Attractors in Rattleback Dynamics, *Uspekhi Fiz. Nauk*, 2003, vol. 173, no. 4, pp. 408–418 [*Phys. Uspekhi*, 2003, vol. 46, no. 4, pp. 393–403].
- [18] Thompson, J. M. T. and Stewart, H. B., *Nonlinear Dynamics and Chaos*, New York: Wiley, 1986.
- [19] Neimark, Yu. I. and Landa, P. S., *Stochastic and Chaotic Oscillations*, Dordrecht: Kluwer, 1992.
- [20] Thurston, W. P. and Weeks, J. R., The Mathematics of Three-Dimensional Manifolds, *Sci. Am.*, 1984, vol. 251, no. 1, pp. 108–120.
- [21] Hunt, T. J. and MacKay, R. S., Anosov Parameter Values for the Triple Linkage and a Physical System with a Uniformly Chaotic Attractor, *Nonlinearity*, 2003, vol. 16, pp. 1499–1510.
- [22] Dmitriev, A. S. and Panas, A. I., *Dynamical Chaos: New Information Carriers for Communication Systems*, Moscow: Fizmatlit, 2002.
- [23] Koronovskii, A. A., Moskalenko, O. I., and Hramov, A. E., On the Use of Chaotic Synchronization for Secure Communication, *Uspekhi Fiz. Nauk*, 2009, vol. 179, no. 12, pp. 1281–1310 [*Phys. Uspekhi*, 2009, vol. 52, no. 12, pp. 1213–1238].
- [24] Bernstein, G. M. and Lieberman, M. A., Secure Random Number Generation Using Chaotic Circuits, *IEEE Trans. Circuits and Systems*, 1990, vol. 37, no. 9, pp. 1157–1164.
- [25] Baptista, M. S., Cryptography with Chaos, *Phys. Lett. A*, 1998, vol. 240, nos. 1–2, pp. 50–54.
- [26] Boltt, E. M. and Meiss, J. D., Targeting Chaotic Orbits to the Moon through Recurrence, *Phys. Lett. A*, 1995, vol. 204, pp. 373–378.
- [27] Schöll, E. and Schuster, H. G., *Handbook of Chaos Control*, New York: Wiley, 2008.
- [28] Andronov, A. A., Vitt, A. A., and Khaikin, S. E., *Theory of Oscillators*, Oxford: Pergamon Press, 1966.
- [29] Kuznetsov, S. P. and Turukina, L. V., Attractors of Smale–Williams Type in Periodically Kicked Model Systems, *Izv. VUZov. Appl. Nonlinear Dynam. (Saratov)*, 2010, vol. 18, no. 5, pp. 80–92 (Russian).
- [30] Benettin, G., Galgani, L., Giorgilli, A., and Strelcyn, J.-M., Lyapunov Characteristic Exponents for Smooth Dynamical Systems and for Hamiltonian Systems: A Method for Computing All of Them: Part 1. Theory; Part 2. Numerical Application, *Meccanica*, 1980, vol. 15, pp. 9–30.

-
- [31] Schuster, H. G. and Just, W., *Deterministic Chaos: An Introduction*, 4th ed., rev. and enl., Weinheim: Wiley-VCH, 2005.
- [32] Kuznetsov, S. P., *Dynamical Chaos*, Moscow: Fizmatlit, 2001 (Russian).
- [33] Kaplan, J. L. and Yorke, J. A., A Chaotic Behavior of Multi-Dimensional Differential Equations, in *Functional Differential Equations and Approximations of Fixed Points*, H.-O. Peitgen and H.-O. Walther (Eds.), Lecture Notes in Math., vol. 730, Berlin: Springer, 1979, pp. 204–227.
- [34] Rayleigh, J. W. S. and Lindsay, R. B., *The Theory of Sound: Vol. 1*, 2nd ed., New York: Dover, 1976.
- [35] Rowland, D. R., Parametric Resonance and Nonlinear String Vibrations, *Amer. J. Phys.*, 2004, vol. 72, pp. 758–766.
- [36] Isaeva, O. B., Kuznetsov, A. S., and Kuznetsov, S. P., Hyperbolic Chaos in Parametric Oscillations of a String, *Nelin. Dinam.*, 2013, vol. 9, no. 1, pp. 3–10 (Russian).
- [37] Isaeva, O. B., Kuznetsov, A. S., and Kuznetsov, S. P., Hyperbolic Chaos of Standing Wave Patterns Generated Parametrically by a Modulated Pump Source, *Phys. Rev. E*, 2013, vol. 87, no. 4, 040901(R), 4 pp.
- [38] Kuptsov, P. V., Kuznetsov, S. P., and Pikovsky, A., Hyperbolic Chaos at Blinking Coupling of Noisy Oscillators, *Phys. Rev. E*, 2013, vol. 87, no. 3, 032912, 7 pp.
- [39] Kuznetsov, S. P. and Sataev, I. R., Hyperbolic Attractor in a System of Coupled Non-Autonomous van der Pol Oscillators: Numerical Test for Expanding and Contracting Cones, *Phys. Lett. A*, 2007, vol. 365, nos. 1–2, pp. 97–104.
- [40] Kuptsov, P. V., Fast Numerical Test of Hyperbolic Chaos, *Phys. Rev. E*, 2012, vol. 85, no. 1, 015203(R), 4 pp.
- [41] Wilczak, D., Uniformly Hyperbolic Attractor of the Smale–Williams Type for a Poincaré Map in the Kuznetsov System, *SIAM J. Appl. Dyn. Syst.*, 2010, vol. 9, pp. 1263–1283.